ELSEVIER

Journal of Chromatography A, 969 (2002) 59–72

JOURNAL OF CHROMATOGRAPHY A

www.elsevier.com/locate/chroma

Effect of moisture on the surface free energy and acid–base properties of mineral oxides

Chenhang Sun, John C. Berg*

Department of Chemical Engineering, University of Washington, Box 351750, Seattle, WA 98195-1750, USA

Abstract

Surface energetic properties of mineral oxides are important in many applications. Since oxide surfaces in practice have generally come in contact with water molecules, it is important to know how water coverage affects the surface properties. In this work, five oxide samples, namely MgO, Al_2O_3, TiO_2, SnO_2 and SiO_2 are heat-treated to various extents, to produce different degrees of hydration, and characterized thereafter by inverse gas chromatography. Water contents of the treated samples are determined independently by Karl Fischer titration, and specific surface areas are measured by the BET method. The results show that in general as water coverage decreases, the Lifshitz–van der Waals component of the specific surface free energy (σ_S^{LW}) increases, but the acid–base interaction potential ($-\Delta G^{AB}$) decreases. These attributes are more sensitive to changes in water coverage at lower coverages, where the surface is presumed to consist of patches of molecular water and unhydrated hydroxyl groups.

Keywords: Surface free energy; Thermodynamic parameters; Acid–base properties; Inverse gas chromatography; Adsorption, water; Oxides

1. Introduction

The surface free energy of solids is an important property in a wide range of situations and applications. It plays an important role in the formation of solid particles either by comminution (cutting, crushing, grinding, etc.) or by their condensation from solutions or gas mixtures by nucleation and growth. It governs their wettability and coatability by liquids, and their dispersibility as fine particles in liquids. It is important in their sinterability and their interaction with adhesives. It controls their propensity to adsorb species from adjacent fluid phases, and influences their catalytic activity. Despite its importance, however, the database for surface energies of solids is small, as compared with that for liquids, and experimental values reported for a given solid may vary by factors as large as two orders of magnitude.

The surface free energy of liquids is readily measurable by direct mechanical means, since it may be taken as identical to the surface tension. For solids, however, any stretching of the interface involves not only a large expenditure of work associated with the elastic and often plastic deformation of the bulk material, but also induces changes in the surface structure. Thus direct mechanical measurement of the surface energy of solids has been achieved only for particular cases. Brittle solids, such as mica and a variety of ionic and covalently bonded crystals (such as diamond) have been cleaved in such a way that surface stretching is avoided, and the work of cleaving yields the surface free energy. For

*Corresponding author. Tel.: +1-206-543-2029; fax: +1-206-543-3778.

E-mail address: berg@cheme.washington.edu (J.C. Berg).

0021-9673/02/$ – see front matter
PII: S0021-9673(02)00231-5

perfectly ductile solids (metals), another direct mechanical method has been devised. At a temperature close to but below the melting point, wires of the metal are loaded with a series of weights. While heavily loaded wires extend, and lightly loaded wires contract (due to surface tension), a load may be found where zero creep occurs, so that again, surface stretching is avoided, and the measured force may be used to determine the surface free energy. For most solids, under most conditions, direct mechanical means are not available.

There are, however, two indirect methods commonly used to assess the surface energy of solids, viz. vapor adsorption measurements using probe vapors [1] and wetting (contact angle) measurements using probe liquids [2]. Contact angle measurements are best suited for low surface energy solids, such as polymers, because for such materials finite contact angles can be achieved using convenient probe liquids. Mineral surfaces, however, are typically wet out (contact angle=0°) by most liquids. Although it is possible to use the ''two liquid approach'' to get a finite contact angle, for example, the contact angle of a high energy solid against water in octane, the resulting information is for the solid–octane interface but not the solid surface itself. However, vapor adsorption measurements, wherein the energy of the physical adsorption of probe vapors against the test solid is determined from the slope of the adsorption isotherm, can conveniently be used to deduce information concerning the surface energetics of higher surface energy materials. Vapor adsorption measurements are effected using inverse gas chromatography (IGC), in which probe vapors are passed over the test solid in particulate form, and the elution trace is used to deduce the slope of the adsorption isotherm.

It is convenient to divide surface energy into the sum of terms representing the different contributions to the intermolecular or interatomic forces which are responsible for it. In particular, one may separate the Lifshitz–van der Waals (LW) component of the surface energy from the contributions due to acid–base self-association, or ionic, covalent or metallic bonding. The LW contribution is primarily due to dispersion force interactions, although small contributions resulting from the presence of permanent dipoles may also be accounted for in this term. It is only the LW contribution to the surface energy which is non-specific and may be taken as intrinsic to the particular material and can thus be used to determine the LW interaction of the surface with another material. The other ''types'' of surface energy are manifested only in the interaction of the surface with probe fluids capable of entering into such interactions. For example, a surface exhibiting acid–base interactions is able to manifest this property in its interaction with acidic or basic probes. A surface exhibiting a metallic bonding contribution to its total surface energy will manifest this aspect of its surface energy only in interacting with liquid metals. Thus, indirect surface energy determinations using probe fluids generally focus principally on the LW contribution. Even this contribution alone may be quite large for mineral surfaces.

Solid surface energy values given by indirect means, such as IGC, are found to differ by more than an order of magnitude from the values obtained by direct mechanical means, such as brittle fracture. For example, the surface energy of MgO {100} face at 25 °C is determined to be 1150 mJ/m^2 by the splitting method [3]. Because {100} is the most stable face of MgO, other faces should have even higher surface energy. However, the surface energy of commercial MgO powders determined by IGC is only ~50 mJ/m^2 [4]. While part of the discrepancy is due to the fact that the IGC measurements yielded only the LW component of the surface energy, a large part of it is also traceable to the presence of an adsorption layer on the mineral surface. An example of this is afforded by mechanical measurements themselves. For example, the surface energy of mica as measured by the mechanical energy required to cleave it in vacuo is 5000 mJ/m^2, as compared with 308 mJ/m^2 for the same material in dry air, 220 mJ/m^2 in air of 50% humidity and 183 mJ/m^2 in water vapor [5]. Similar results were reported for silver wires from zero creep experiments at 1205 K in oxygen. In vacuum, the surface energy was measured at 1140 mJ/m^2, while at an O_2 partial pressure of 0.08 mmHg, it was 980 mJ/m^2, and at 150 mmHg, 350 mJ/m^2 [6] (1 mmHg=133.322 Pa).

Highly polar adsorbates, in particular water, are strongly adsorbed on oxide surfaces because it is energetically favorable to terminate ionic solids with a polar molecule which can be oriented to neutralize surface electric fields, rather than to abruptly termi-

nate the crystal with a layer of ions in normal lattice positions, leaving intense fields directed into space. Both experimental evidence [7–9] and molecular dynamic simulations [10,11] have shown that when a clean surface is in contact with humid air, dissociative adsorption of water (dissociated into hydroxyl and proton) happens first around surface defects. Molecular adsorption becomes dominant as monolayer coverage is approached, and more water can be loosely adsorbed on top of this first layer through hydrogen boding. The oxide samples used in IGC measurements are often prepared in the powder form as hydroxide, carbonate and oxalate, and then decomposed to form oxide which is inevitably hydrated. The surface properties determined on such materials therefore correspond to a clean surface covered by hydroxyl groups and molecular water. Although strictly speaking these are not characteristics of a ''pure'' surface, from a practical point of view, they are fair representations of the surfaces of everyday-use materials.

Oxide particles are widely used in industry as catalysts, fillers, coating materials, pigments and adsorbents. Their surface properties, especially their surface energetics, are highly useful information for understanding their structure, improving their performance in various applications and finding new applications. Depending on the specific application, oxide particles are usually treated before usage. The pretreatment process, in most cases heating, may strongly affect surface energy and chemistry by changing water coverage or even modifying solid crystal structure. Papirer et al. studied the effect of heating on the surface free energy and acid–base properties of several mineral oxides including silica (both crystalline and amorphous) [12,13], γ-alumina [14] and hematite [15]. The samples were preheated at various temperatures from 60 to 700 °C. It was found that except for crystalline silica, the LW component of solid surface free energy (σ_S^{LW}) of all other materials increased with preheating temperature until a certain temperature (ranging from 200 to 500 °C), then decreased, while the acid–base interaction potential ($-\Delta G^{AB}$) upon adsorption of acid–base probes decreased first, then increased. Crystalline silica samples, on the other hand, did not show a uniform trend of changes in σ_S^{LW} and $-\Delta G^{AB}$. For amorphous silica, the authors attributed the initial increase of σ_S^{LW} to the loss of physisorbed water and the formation of highly strained tri-siloxane rings resulting from the condensation of surface hydroxyl groups. The decrease of σ_S^{LW} at still higher treatment temperatures was attributed to the formation of less-strained tetra-siloxane rings, due to surface reconstruction. For alumina, they speculated that a layer of boehmite ($Al_2O_3 \cdot H_2O$) had been formed on the surface, due to previous contact with humid air, and the transformation of boehmite back to γ-alumina upon heating caused the changes in σ_S^{LW} and $-\Delta G^{AB}$. Although the authors realized the importance of water adsorption on the oxide surface, they did not measure or account for the amount of water desorbed during the process of heating until in a recent study of hematite, in which they applied the technique of temperature programmed desorption (TPD). In that work, a correlation between the rate of water desorption and the surface free energy of hematite was proposed. However, a correlation between water/hydroxyl coverage with surface energy would be more plausible. TPD has two apparent shortcomings: firstly, it monitors only the amount of water desorbed; secondly, it does not distinguish physisorbed water from water formed by hydroxyl condensation. So far no work appears to have been reported directly correlating molecular water coverage to surface properties for mineral oxides. When the heating temperature is high enough for complete dehydration, it may also be high enough for surface reconstruction. Considering that in practice only a few applications require such high temperature calcination, the effect of moderate preheating may be of more practical significance.

The objective of this work is to explore how moderate temperature heat-treatment (50 to 220 °C) influences surface energy and chemistry of mineral oxides. Five oxides, namely MgO, Al_2O_3, TiO_2, SnO_2 and SiO_2 are studied. Their source information and specifications are shown in Table 1. Using inverse gas chromatography (IGC), their surface energy is characterized in terms of their Lifshitz–van der Waals energy component (σ_S^{LW}), while their surface acid–base properties are characterized by the acid–base contribution to the free energy change ($-\Delta G^{AB}$) upon adsorption of an acid or base probe vapor. In addition, specific areas and molecular water contents of the treated samples are measured by the

Table 1
Source data for the oxides used in this study

Oxide	Manufacturer	Specifications
Al_2O_3	Aldrich	Purity 99.5%, α phase, $d \leq 45$ μm
MgO	Aldrich	Purity >99%, fused, $d \leq 425$ μm
SiO_2	Geltech	Purity 99.9%, $d \leq 45$ μm
SnO_2	Aldrich	Purity 99.9%, $d \leq 45$ μm
TiO_2	J.T. Baker	Purity 99.9%, anatase phase

BET technique [16] and Karl Fischer titration [17], respectively, such that molecular water coverage of the surface can be determined independently. Based on the experimental data, a correlation between water coverage and surface properties is made.

2. Experimental

2.1. IGC measurements

2.1.1. Equipment

A Varian 3400 gas chromatograph (Varian, Walnut Creek, CA, USA) equipped with dual high-sensitivity flame ionization detection (FID) systems was used for the IGC measurements. The injector and detector temperatures were set to 175 and 250 °C, respectively. Dry nitrogen was used as the carrier gas, with a flow-rate of 30 ml/min. PTFE tubing, 5 mm diameter, was used for the columns. An appropriate amount of oxide (total surface area about 2 m^2) was packed in the column and stabilized by glass wool at the two ends. The packed column was preheated in dry N_2 at the desired treatment temperature for 24 h and then cooled down to 50 °C for IGC measurements.

2.1.2. Materials

High-purity (>99.5%) oxide powders were purchased from J.T. Baker and Aldrich and used as received. High-purity (>99%) methane provided by Alltech Associates was used as the non-adsorbing reference probe gas. HPLC-grade linear alkanes (pentane to decane) were used as non-specifically adsorbing probes. Acetone and chloroform were used as basic and acidic probes, respectively. These solvents were all purchased from Aldrich. The molar areas (a_{mol}) of the alkanes were determined by assuming that each CH_2 group occupies 0.06 nm^2 and each CH_3 group occupies 0.08 nm^2, as suggested by Dorris and Gray [18]. The molar areas of chloroform and acetone were estimated from their liquid molar volume v_{mol} by assuming a spherical molecular shape and hexagonal packing [19]:

$$a_{mol} = 1.33\, N^{(1/3)}\, v_{mol}^{(2/3)} \quad (1)$$

where N is Avogadro's number. The vapor pressures of all the probes at 50 °C were calculated using handbook formulations of Antoine's equation (see Ref. [20]). The properties of the probe fluids are listed in Table 2.

2.1.3. Operation and data analysis

IGC was operated in the infinite dilution regime, which corresponds to very low surface coverage by the adsorbates. To achieve this, samples of less than 1 μl of probe vapor were injected into the stationary phase column with a Hamilton syringe. Retention times of all probes were computed by the ''first moment method'':

$$t_R = \frac{\int f(t) t \, dt}{\int f(t) \, dt} \quad (2)$$

where $f(t)$ represents the elution curve profile. The relative retention time, $t'_R = t_R - t_0$, where t_0 is the

Table 2
Properties of probe fluids

	Boiling point[a] (°C)	Vapor pressure[b] (mmHg)	Molar area[c] (m^2/mol)
Pentane	36.1	1193.8	2.047×10^5
Hexane	68.7	405.3	2.408×10^5
Heptane	98.4	141.6	2.769×10^5
Octane	125.7	50.4	3.130×10^5
Nonane	150.8	19.1	3.492×10^5
Decane	174.1	7.4	3.853×10^5
Acetone	56.2	614.8	2.022×10^5
Chloroform	61.2	519.6	2.091×10^5

[a] Handbook of Chemistry and Physics, 71st ed., CRC Press, Boca Raton, FL, 1990 [24].
[b] Calculated by Antoine's vapor pressure correlation [20], at 50 °C.
[c] Molar areas of linear alkanes are computed in accord with the method of Dorris and Gray [18], and those of acetone and chloroform are computed using Eq. (1).

retention time of the non-adsorbing reference probe (methane), is used to obtain the relative retention volume, V_N, defined as the volume of carrier gas required to elute the adsorbing probe:

$$V_N = jt'_R v \quad (3)$$

where v is the volumetric flow-rate of the carrier gas, and j is the James–Martin correction factor used to correct for the pressure drop across the column (see Ref. [21]). The relative retention volume of an adsorbing probe is directly related to the slope of its adsorption isotherm, K:

$$V_N = KA_{tot} \quad (4)$$

where A_{tot} is the total area of the adsorbent in the column. The constant K is related to the standard free energy of adsorption, $-\Delta G^0_{ads}$, in accord with

$$RT \ln V_N = -\Delta G^0_{ads} + C_1 \quad (5)$$

where C_1 is a constant dependent upon the choice of standard state for adsorbed and vapor species and the total area in the column. For any non-specifically adsorbing probe, it is related to the surface energies in accord with:

$$-\Delta G^0_{ads} = 2a_{mol}(\sigma_S^{LW}\sigma_L^{LW})^{1/2} + C_2 \quad (6)$$

where σ_S^{LW} is the LW component of the solid surface free energy, σ_L^{LW} is the LW component of the probe liquid surface tension, a_{mol} is the molar area of the adsorbate on the surface and C_2 is a constant accommodating the choice of standard state. Combining Eqs. (4)–(6):

$$RT \ln V_N = 2a_{mol}(\sigma_S^{LW}\sigma_L^{LW})^{1/2} + C \quad (7)$$

Thus a plot of $RT \ln V_N$ against $a_{mol}(\sigma_L^{LW})^{1/2}$ for a series of apolar probes (such as normal alkanes) should yield a straight line (the ''alkane line'') whose slope is $2(\sigma_S^{LW})^{1/2}$ as shown in Fig. 1a for the case of TiO_2 preheated at 50 °C, such that σ_S^{LW} can be determined.

The acid–base properties of a surface are characterized by the acid–base contribution to the free energy change upon adsorption, $-\Delta G^{AB}$, of chloroform (acid probe) and acetone (base probe). The larger $-\Delta G^{AB}$ of chloroform is, the stronger the basicity of the surface, and conversely, the larger

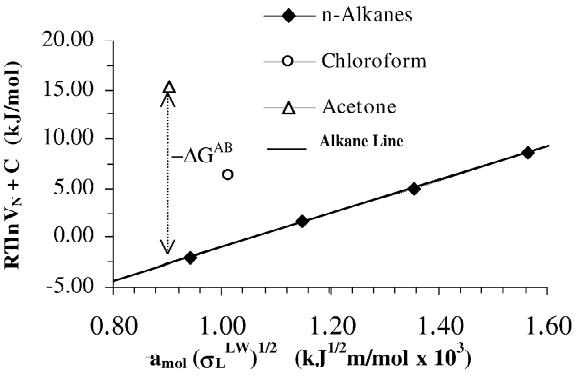

(a)

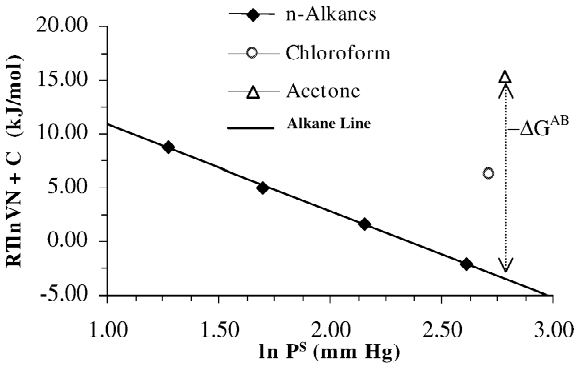

(b)

Fig. 1. Determination of σ_S^{LW} and $-\Delta G^{AB}$ of TiO_2 preheated at 50 °C by inverse gas chromatography (IGC). (a) The molar area approach, (b) the vapor pressure approach.

$-\Delta G^{AB}$ of acetone, the stronger the acidity of the surface. After obtaining the retention volume of the acid or base probe, two approaches are available to process the data to determine $-\Delta G^{AB}$. The first one is the molar area method in which $-\Delta G^{AB}$ is calculated according to:

$$RT \ln V_N = 2a_{mol}(\sigma_S^{LW}\sigma_L^{LW})^{1/2} - \Delta G^{AB} + C \quad (8)$$

As shown in Fig. 1a, the displacement of the acid–base probe above the alkane line corresponds to $-\Delta G^{AB}$. The difficulty using Eq. (8) is that one must estimate the molar area of the acid–base probe on the surface, which is subject to ambiguity. Another approach is the vapor pressure method in

which one plots RT ln V_N against ln P^S of all the probes, where P^S is the vapor pressure of the probe. A straight alkane line is usually formed, and again, the displacement of the acid–base probe above the alkane line corresponds to a representative value of $-\Delta G^{AB}$, as shown in Fig. 1b.

All the five samples, MgO, Al_2O_3, TiO_2, SnO_2 and SiO_2, were preheated in the column with dry N_2 flowing through at 50, 105, 140, 180 and 220 °C, respectively, for 24 h before measurement, and as noted above, all measurements were carried out at 50 °C.

2.2. Karl Fischer titration

2.2.1. Materials and reaction

Water content determination was achieved by Karl Fischer titration. Karl Fischer reagent was purchased from J.T. Baker. It is composed of four components: iodine, sulfur dioxide, pyridine and methanol, serving as solvent. Pure methanol purchased from Aldrich was used as the working medium. In the presence of water, sulfur is oxidized from valence 4 to valence 6, and iodine is reduced to iodide according to Ref. [17]:

$$H_2O + I_2 + [PyH]SO_3CH_3 + 2Py \rightarrow 2[PyH]I + [PyH]SO_4CH_3 \quad (9)$$

The titer of KF reagent was determined by a water in methanol standard solution, which was purchased from Sigma. Note that Karl Fischer titration is sensitive only to molecular water, either adsorbed or in solution, but not to hydroxyl groups on the mineral surface.

2.2.2. Operation

All titrations were carried out in a sealed vessel, and all oxide samples were treated under exactly the same conditions as they were treated for IGC measurements. Before a solid sample was introduced into the vessel, methanol was introduced and pre-titrated to ensure a water-free environment. At least 3 min were given for complete water extraction from samples before titration was started.

Even though Karl Fischer titration is self-indicating (from yellow to dark brown when the end-point is reached), a more reliable instrument indication was applied. This employed two platinum electrodes which were placed in the solution to be titrated. A constant voltage of 500 mV was applied between the electrodes. When water is present, no excess iodine exists, and the redox reactions

$$I^- \rightarrow e^- + 1/2I_2 \text{ at cathode}$$

$$1/2I_2 + e^- \rightarrow I^- \text{ at anode}$$

do not occur. However, after all water molecules are consumed, and excess iodine appears, the redox reactions do occur and produce a current between the two electrodes. The potential difference between these two electrodes drops from 500 mV to nearly zero. Titration is considered complete when the reading remains stable for at least 20 s. The experimental error is believed to be within ±0.05 mg water.

In order to verify the Karl Fischer titration results, thermogravimetric analysis (TGA) was performed for Al_2O_3 and MgO. In the TGA measurements, samples were put into the sample holder and heated in dry N_2 flow. The mass was measured as a function of heating time and temperature. Although TGA cannot provide information about the total water present in the sample, the amount of water removed at each heating stage can be determined by assuming that all mass loss resulted from dehydration.

2.3. Surface area measurement

Surface area was obtained by the BET (Brunauer–Emmett–Teller) method, using nitrogen. The measurements were carried out with a Flowsorb II 2300 Surface Area Analyzer (Micromeritics, Norcross, GA, USA). Again, all samples were treated as they were for IGC measurements and KF titration. The experimental error is believed to be within ±2%.

3. Results and discussion

3.1. Surface energy: σ_S^{LW}

The elution behavior of a probe gas going through a GC column is controlled mainly by the interactions between the probe molecules and the solid sample packed in the column. Thus one can infer infor-

mation about the effect of heat-treatment of the solid surface by examining the elution profiles of the same probe on surfaces treated at different temperatures. The elution profiles of heptane through the SiO_2 column are shown in Fig. 2. It is to be noted that the retention peak was originally symmetric, but as preheating temperature increased, the peak became broader and more skewed. This trend was not unique to the heptane–SiO_2 system, but was observed to some extent for all alkanes with all five oxides examined.

Since operations were carried out in the infinite-dilution regimes, the ''sorption effect'' [21] is assumed to be negligible. A more plausible explanation for the peak tailing is surface energetic heterogeneity. When the probe gas is injected into the column, the initial input peak is symmetric, and if the surface is homogeneous, the output peak will also be symmetric, but wider and flatter. The stronger the interaction between gas and solid, the wider and flatter the output peak. Considering a heterogeneous surface that is composed simply of two kinds of sites, high-energy and low-energy sites, it is evident that probe molecules interacting with the low-energy sites will generate a narrower and sharper peak, whereas those interacting with the high-energy sites will generate a wider and flatter peak. The final output is a summation of the two, which is not symmetric, as illustrated in Fig. 3. The more heterogeneous the surface, the less symmetric the peak is. Pure oxide surfaces should be strongly heterogeneous because of different crystal surfaces exposed and lattice defects. The adsorbed water layer will cover all these features and tend to make the surface smoother and nearly homogeneous. The fact that elution profiles of alkanes turn increasingly skewed as preheating temperature is increased corroborates this assumption.

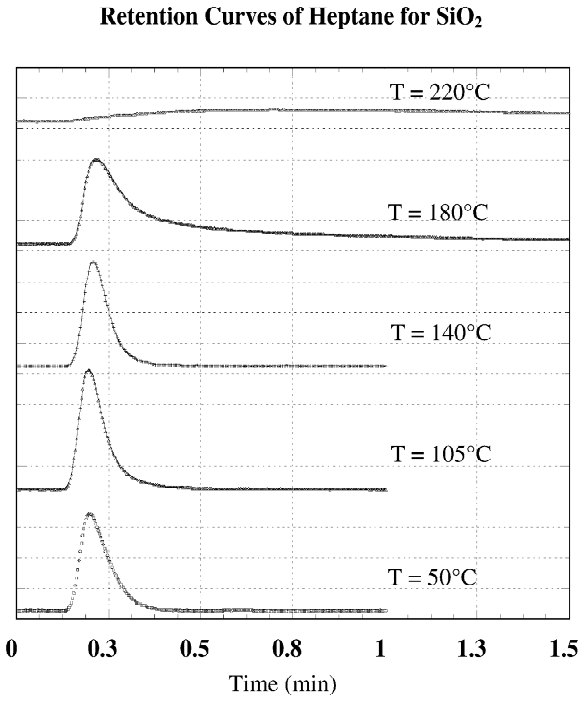

Fig. 2. Retention profiles of heptane on SiO_2 samples heat-treated at different temperatures (T). All IGC measurements were carried out at 50 °C. Although only the data obtained before 1.5 min are shown for the 220 °C curve, actual measurement was carried on until the baseline was reached.

The straightness of the alkane line in each case is an assurance of the validity of the assumptions inherent in Eq. (7). Lines with very high linear regression coefficients (>0.995) were indeed formed in most cases. However, for TiO_2, when the surface was preheated at 180 and 220 °C, the alkane lines bent significantly downward, as shown in Fig. 4. A possible cause of bending of the alkane line would be the use of incorrect molar areas for the probes. If heptane and octane (the last two points on the alkane line of 220 °C) actually occupy less area on the surface than the value used, these two points should be shifted to the left, and a straight line may be formed. However, for linear alkanes that interact only with other materials through LW interactions, the best way to minimize potential energy upon adsorption is to lie flat on the surface to maximize

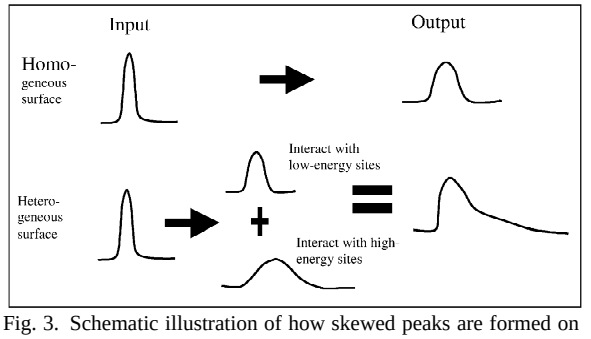

Fig. 3. Schematic illustration of how skewed peaks are formed on heterogeneous surfaces.

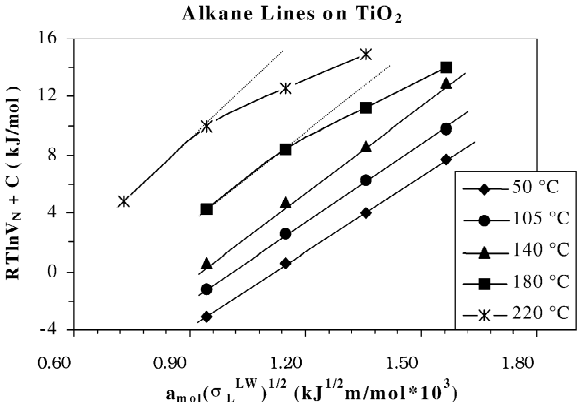

Fig. 4. Alkane lines for TiO_2. They are seen to be straight when the surface is heat-treated at low temperatures but bend downward when the pretreatment temperature is high.

the interaction area. Since the interactions between probe molecules and the solid surface become stronger as preheating temperature increases, it appears that the actual molar area should increase rather than decrease.

Such an effect may be produced by different accessibility of the probes to the surface. Fig. 5 shows schematically the situation when a pentane molecule and an octane molecule are adsorbed onto a porous oxide surface. If the surface is preheated at low temperature, there is still enough water left to make the surface smooth such that the whole surface is accessible to both pentane and octane. However, as the preheating temperature is increased and more water is driven off, micropores may appear. Some of these pores may be accessed by pentane but not by octane, because of its larger size. Therefore, the effective column octane passes through is shorter than that pentane passes through, so that the retention time of octane is less than expected. If different accessibility is the cause of the curved alkane line, one would expect TiO_2 to have relatively high surface area and a significant change in water coverage upon heating. This is seen to be the case.

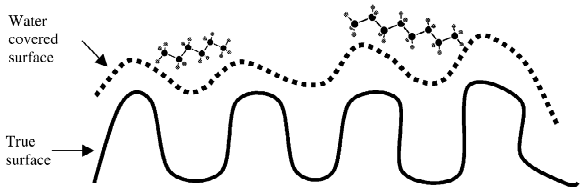

Fig. 5. Schematic representation of the adsorption of pentane and octane on a water-covered solid surface. When the water coverage is high enough, the whole surface is accessible to both pentane and octane. After the surface is heated at a high enough temperature, some micropores, which are not accessible to octane, will be exposed.

Typically, a good, straight line is observed using the series from pentane to nonane, which enables one to make a comfortable calculation of σ_S^{LW}. However, if one keeps adding higher alkanes, such as decane, undecane, dodecane, tridecane, etc., eventually a point is reached where the alkane line starts to bend downward, either because of incomplete elution or different probe accessibility. For TiO_2 preheated at 180 and 220 °C, the bending occurs earlier. While accurate calculation is impossible with a curved alkane line, one can still estimate σ_S^{LW} by using only the points for the linear alkanes that do form a straight line.

σ_S^{LW} values for the five oxides measured at 50 °C as a function of preheating temperature are listed in Table 3. One can see that as a general trend, the non-specific surface free energy increases with preheating temperature. This is what would be expected, since σ^{LW} of water (21.1 mJ/cm^2) is much lower than that of a typical solid surface. As preheating temperature increases, more water is driven from the

Table 3
The LW component of surface free energy of the five oxides pretreated at different temperatures, measured at 50 °C. In mJ/m^2

Treating T	Al_2O_3	MgO	SiO_2	SnO_2	TiO_2
50 °C	61.6±1.2	38.6±0.6	43.5±3.4	67.3±3.4	74.1±1.8
105 °C	68.4±3.0	54.6±2.4	62.1±2.1	72.5±5.9	79.2±2.4
140 °C	70.1±2.7	56±2.5	62.6±4.0	71.4±4.9	98.5±2.6
180 °C	92±4.3	55.6±2.6	79.6±17.6	81.2±7.0	100.8[a]
220 °C	100.4±5.9	73.9±10	105.9±23	86.9±1.6	144.1[a]

[a] Error missing due to inadequate experimental points to specify the alkane line.

surface such that the probe molecules can interact with the bare surface more easily. These results agree qualitatively with those given by Ligner et al. [12]. However, quantitative comparison is unrealistic because samples tested were of different origin, and the experimental conditions were not equal.

3.2. Acid–base properties: $-\Delta G^{AB}$ for acetone and chloroform

Chloroform and acetone were used as acid–base probe molecules. Chloroform is a nearly mono-functional acidic molecule, so that $-\Delta G^{AB}$ for chloroform on a surface is a good measure of the basic strength of that surface. Acetone, on the other hand, is predominantly basic, although it is believed to possess non-negligible acidic functionality as well. Thus $-\Delta G^{AB}$ for acetone on a surface represents primarily the acidic strength of that surface. What needs to be emphasized is that $-\Delta G^{AB}$ values measured are not intrinsic properties of the solid itself but depend on the properties of the adsorbate as well. In order to compare the acid–base properties of two surfaces, one can only use $-\Delta G^{AB}$ values of the same probe on them.

The elution profiles for chloroform and acetone are examined first. Unlike those of the alkanes, all the acid–base probe peaks are skewed, even when the surface is preheated only at 50 °C. This clearly indicates the existence of surface heterogeneity in terms of the ability to interact with probe molecules through acid–base interactions. As preheating temperature increases, the AB probe peaks also turn wider and more skewed than do the alkane peaks, suggesting that the overall heterogeneity of the surface increases.

The results of $-\Delta G^{AB}$ for acetone and chloroform on the five oxide surfaces determined by both the molar area approach and the vapor pressure approach are shown in Table 4. It is to be noted that negative values of $-\Delta G^{AB}$ were observed for chloroform when the surfaces were preheated at 180 and 220 °C. These are not physically realistic, and should be interpreted as values near zero. If one is interested only in the changes of $-\Delta G^{AB}$ upon heating, the data provide a basis for such a comparison. From Table 4, one can see that as a general trend, $-\Delta G^{AB}$-values for both acetone and chloroform decrease as preheating temperature increases, i.e. as water is removed. The acid–base properties of oxides with respect to their interaction with vapor components thus appears to be largely a function of the molecular water adsorbed on their surfaces. These results agree qualitatively with those given by Papirer and co-workers [12–15].

3.3. Surface area and water content

The surface area of the oxides, as determined by the BET method, are shown in Table 5. It is seen that as the heat-treatment temperature increases, the surface area of these oxides also increases slightly.

The results of water content determinations are shown in Table 6 both in terms of mg (water)/g (oxide) and equivalent monolayer coverage. The latter values are obtained from the measured BET area and assuming eight water molecules per nm^2 of surface, in accord with Eq. (1). It is to be noticed that no molecular water could be detected on SiO_2 after the sample was heat-treated above 140 °C, which is consistent with Hair's conclusion that the removal of adsorbed water on SiO_2 surface can be achieved by prolonged evacuation at temperatures of 150 °C and above [22], and Nishioka's conclusion that water desorbed above 150 °C can be wholly accounted for as the product of the dehydroxylation of surface silanols [23].

Thermogravimetric analysis (TGA) was also performed for Al_2O_3 and MgO. The comparison between the results of TGA and Karl Fischer titration is shown in Table 7. In both cases, the water content change given by Karl Fischer titration is somewhat higher than that given by TGA. This is reasonable, because in TGA measurements, samples at the bottom of the sample holder may not be sufficiently well exposed to the dry N_2 flow. However, in Karl Fischer titration, all samples are fully dehydrated.

3.4. Effect of water coverage on σ_S^{LW} and $-\Delta G^{AB}$

Values of σ_S^{LW} and $-\Delta G^{AB}$ for Al_2O_3, MgO, SiO_2, SnO_2 and TiO_2 are plotted against water coverage in Figs. 6 and 7, respectively. From these figures, one sees that decreasing water coverage results in increasing σ_S^{LW} but decreasing $-\Delta G^{AB}$. What is interesting is that the changes appear to

Table 4
AB properties of the oxides preheated at different temperatures

	$-\Delta G^{AB}$ of chloroform (kJ/mol)		$-\Delta G^{AB}$ of acetone (kJ/mol)	
	Molar area method	Vapor pressure method	Molar area method	Vapor pressure method
Al_2O_3, 50 °C	3.1±0.3	4.9±0.3	14.3±0.4	15.0±0.4
105 °C	5.0±0.5	6.9±0.6	15.2±0.5	15.9±0.6
140 °C	0.1±0.5	2.1±0.5	11.6±0.5	12.3±0.6
180 °C	−2.2±0.6	0.1±0.8	6.9±0.6	7.7±0.8
220 °C	−3.5±0.8	−1.0±1.0	7.5±0.8	8.4±1.0
MgO, 50 °C	3.8±0.6	5.3±0.6	12.6±1.6	13.2±1.6
105 °C	4.2±0.7	6.0±0.7	13.9±1.2	14.7±1.2
140 °C	2.6±1.7	4.6±1.7	16.3±1.1	17.1±1.1
180 °C	−0.6±0.6	1.2±0.7	10.1±0.8	10.8±0.8
220 °C	−3.3±1.7	−1.3±2.1	7.2±1.6	7.9±2.1
SiO_2, 50 °C	0.7±1.0	2.5±0.9	16.6±1.0	17.5±0.9
105 °C	0.3±0.5	2.2±0.5	15.6±0.6	16.4±0.6
140 °C	1.9±0.9	3.8±0.9	17.1±0.8	17.9±0.9
180 °C	−3.3±2.8	−1.1±3.4	10.6±2.6	11.4±3.4
220 °C	−4.1±3.2	−1.6±4.0	8.5±3.1	9.4±4.0
SnO_2, 50 °C	1.2±0.7	3.1±0.7	16.7±0.6	17.4±0.7
105 °C	1.5±1.2	3.5±1.3	15.1±1.1	15.8±1.2
140 °C	1.3±1.1	3.3±1.1	15.9±0.9	16.7±1.0
180 °C	1.2±1.2	3.4±1.4	11.5±1.4	12.2±1.7
220 °C	−3.2±0.3	−1.0±0.4	10.0±0.3	10.8±0.3
TiO_2,50 °C	7.1±0.3	9.2±0.3	18.1±0.3	18.9±0.3
105 °C	7.9±0.4	10.1±0.4	18.8±0.4	19.7±0.4
140 °C	7.8±0.4	10.3±0.4	19.8±0.4	20.8±0.4
180 °C	6.4[a]	8.7[a]	15.3[a]	16.1[a]
220 °C	0.9[a]	3.8[a]	9.9[a]	10.9[a]

[a] Error missing due to inadequate experimental points to specify the alkane line.

occur in two stages, as indicated by the dashed lines. During the first stage (the right side) when water coverage is higher than a certain value, σ_S^{LW} and $-\Delta G^{AB}$ do not change markedly. However, after that value is passed (the left side), σ_S^{LW} and $-\Delta G^{AB}$ become much more sensitive to changes in water coverage. Although it is difficult to locate the transition point precisely with only five data points, the trend is clear. This observation may be rationalized as follows. Both experimental evidence and molecular dynamic simulations have shown that when a clean surface is in contact with humid air, dissociative adsorption of water (dissociated into hydroxyl and proton) happens first around surface defects in order to increase the coordination number of atoms at the defects. Molecular adsorption becomes dominant as monolayer coverage is approached, and more water can be loosely adsorbed on top of this first layer through hydrogen bonding. However, de Leeuw and Parker have shown that on MgO and CaO {100} surfaces, 100% hydroxylation is energetically very unfavorable, and a 75% hy-

Table 5
Surface area of the oxides after preheating, in m^2/g

	Al_2O_3	MgO	SiO_2	SnO_2	TiO_2
No heating	10.05	1.03	3.05	6.84	7.7
50 °C	10.05	1.03	3.05	6.84	7.7
105 °C	10.24	1.05	3.14	6.84	8.07
140 °C	10.28	1.05	3.19	7.04	8.23
180 °C	10.28	1.07	3.02	6.96	8.33
220 °C	10.67	1.12	3.19	7.18	8.62

Table 6
Water content of oxides after heating at different temperatures in terms of mg (water)/g (oxide) and equivalent monolayers

	Water content (mg (water)/g (oxide))					Water content (equivalent monolayers)				
	Al_2O_3	MgO	SiO_2	SnO_2	TiO_2	Al_2O_3	MgO	SiO_2	SnO_2	TiO_2
No heating	5.45±0.05	8.42±0.05	0.72±0.05	1.65±0.05	3.87±0.05	2.27±0.02	34.2±0.2	0.99±0.05	1.01±0.02	2.10±0.02
50 °C	1.53±0.05	5.13±0.05	0.71±0.05	1.30±0.05	1.22±0.05	0.64±0.02	20.8±0.2	0.97±0.05	0.79±0.02	0.66±0.02
105 °C	1.32±0.05	4.33±0.05	0.36±0.05	1.10±0.05	0.88±0.05	0.54±0.01	27.2±0.2	0.48±0.05	0.67±0.02	0.46±0.02
140 °C	1.11±0.05	3.57±0.05	–	0.90±0.05	0.77±0.05	0.45±0.01	14.2±0.2	–	0.53±0.02	0.39±0.02
180 °C	0.87±0.05	3.40±0.05	–	0.80±0.05	0.66±0.05	0.35±0.01	13.3±0.2	–	0.48±0.02	0.33±0.02
220 °C	0.70±0.05	3.15±0.05	–	0.56±0.05	0.27±0.05	0.27±0.01	11.8±0.1	–	0.33±0.02	0.13±0.02

droxyl coverage provides the lowest total hydration energy [11]. Therefore, after 75% hydroxylation is reached, water molecules further adsorbed may no longer dissociate, but retain their molecular form. It is also shown for TiO_2 that the most stable configuration at monolayer coverage is one containing both dissociated water (hydroxyl groups) and molecular water [10]. This may be true for other oxide surfaces as well. Since Karl Fischer titration can detect only molecular water, the water coverage shown in Figs. 6 and 7 is ''molecular water coverage''. Even after all molecular water is removed by the Karl Fischer reagent, surface hydroxyl groups remain. With the exception of MgO and SiO_2, the ''critical coverage'' of Al_2O_3, SnO_2 and TiO_2 are all at sub-monolayer level. It is possible that for these three oxides, the critical water coverage corresponds to a point where the combination of molecular water and hydroxyl groups provides a full monolayer coverage on the surface. When the total coverage is lower than that of a full monolayer, the removal of water will result in exposure of bare surface and thus greatly affect the apparent energetic properties. For MgO, the results suggest that multilayer water patches are formed before the surface is fully covered. MgO is known to be highly hygroscopic. For SiO_2, such a transition point cannot be identified. The increase in σ_S^{LW} after all molecules are removed is very likely due to the formation of siloxane groups resulting from condensation of hydroxyl groups.

By extending the dashed lines in Fig. 6 to zero water coverage, σ_S^{LW} of the dry but still hydroxylated oxides can be estimated to be 155 mJ/m^2 for Al_2O_3, 160 mJ/m^2 for MgO, 70 mJ/m^2 for SiO_2, 112 mJ/m^2 for SnO_2 and 170 mJ/m^2 for TiO_2, and if one extends the dashed lines toward higher water coverage, eventually σ_S^{LW} will decrease to approximately the LW component of the surface tension of water. This will occur at several equivalent monolayers, when the solid surface is totally masked by the water adlayer.

4. Conclusion

Five mineral oxides have been heat-treated in dry nitrogen at different temperatures to produce different levels of adsorbed water. Their surface energetic properties were measured by inverse gas chromatography at infinite dilution, while their water contents were determined by Karl Fischer titration, and the specific surface areas measured using the BET method. The results show that in general as water coverage decreases, oxide surfaces become ener-

Table 7
Comparison between TGA results and KFT results

	MgO	Al_2O_3
TGA	Heated at 250 °C for 24 h Mass loss: 4.81 mg/g	Heated at 220 °C for 24 h Mass loss: 4.12 mg/g
KFT	Heated at 220 °C for 24 h Water content change: 5.27 mg/g	Heated at 220 °C for 24 h Water content change: 4.75 mg/g

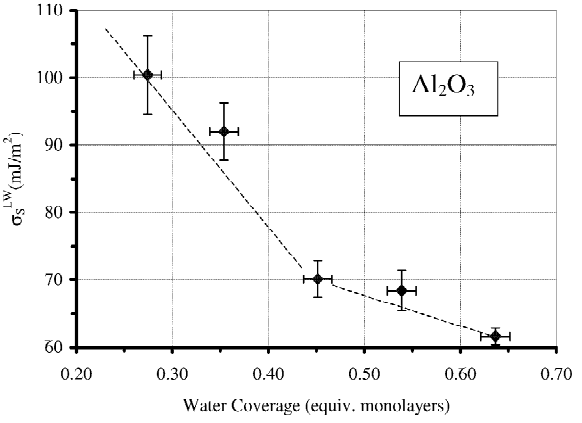

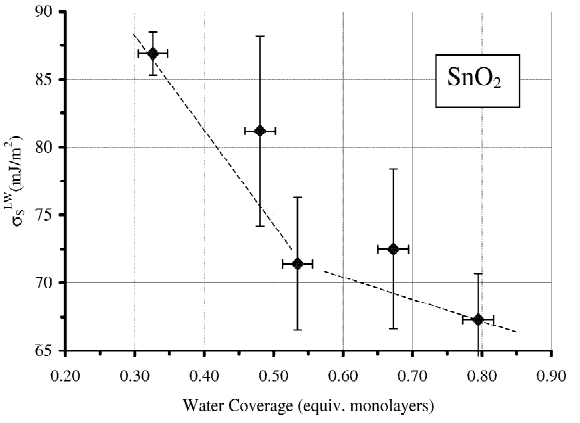

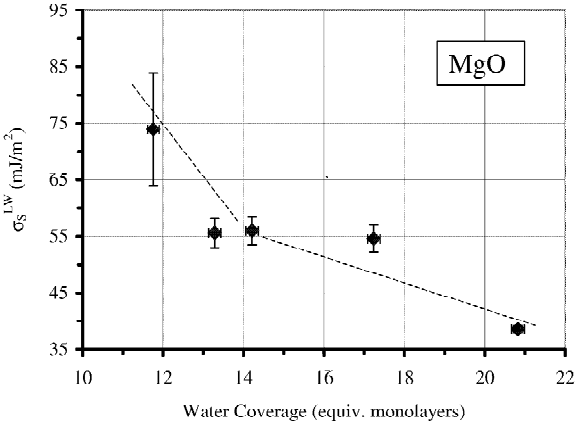

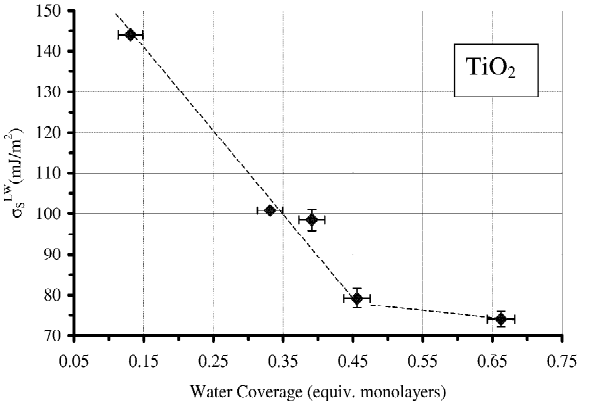

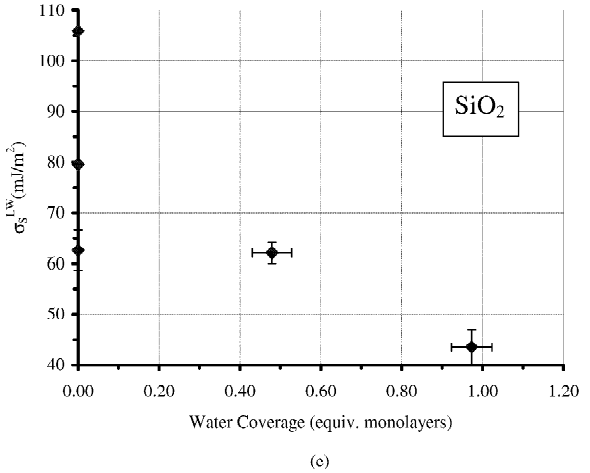

Fig. 6. σ_S^{LW} (in mJ/m^2) of (a) Al_2O_3, (b) MgO, (c) SnO_2, (d) TiO_2, and (e) SiO_2 against water coverage.

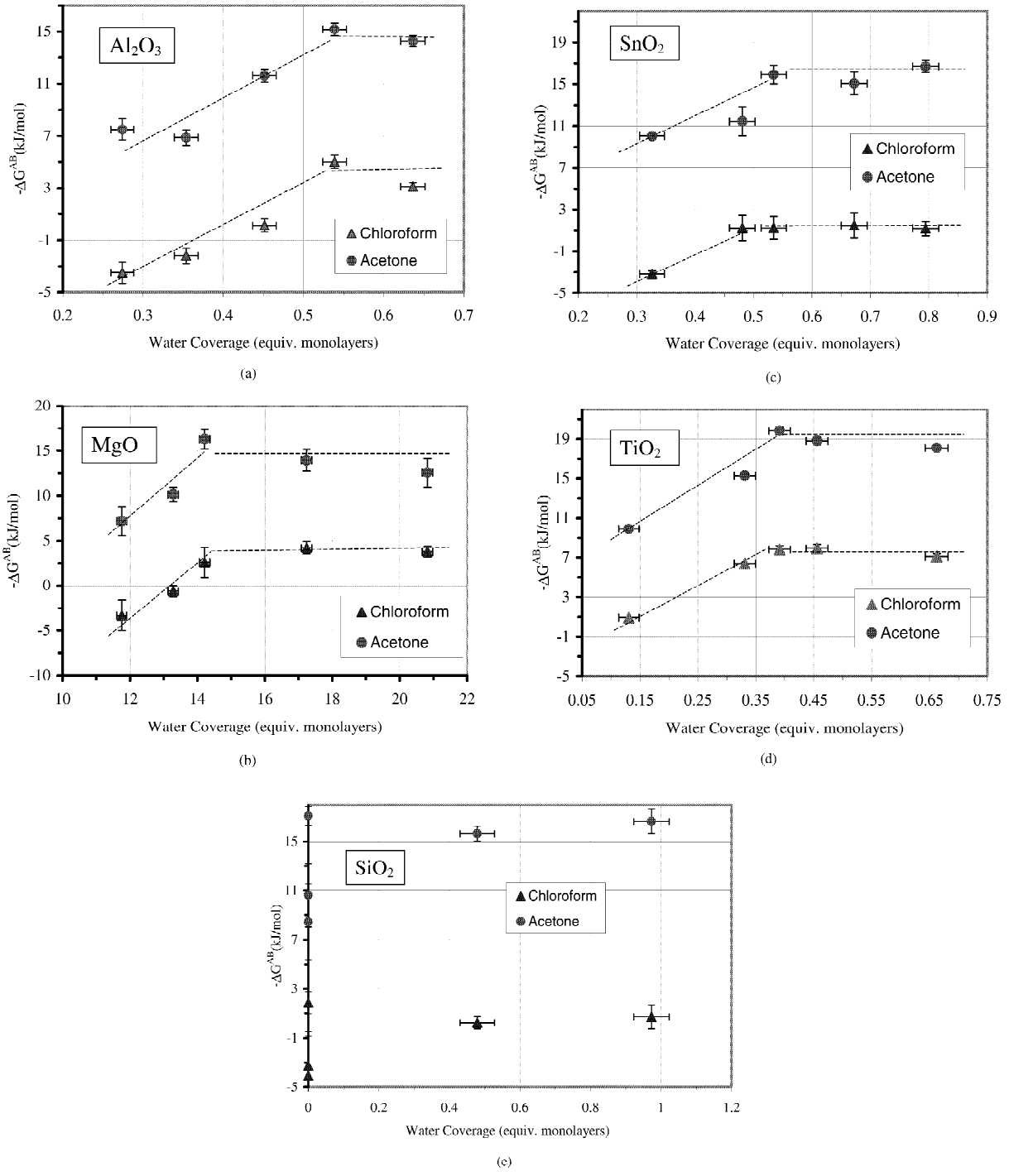

Fig. 7. $-\Delta G^{AB}$ for adsorption of acetone (base probe) and chloroform (acid probe) onto (a) Al_2O_3, (b) MgO, (c) SnO_2, (d) TiO_2, and (e) SiO_2 against water coverage. Data shown were determined by the vapor pressure approach.

getically more heterogeneous. The Lifshitz–van der Waals component of surface energy (σ_S^{LW}) increases and the acid–base interaction potential ($-\Delta G^{AB}$) decreases. This is because compared with water, bare oxide surfaces have higher surface energy but weaker acid–base interaction ability. These values are particularly sensitive to changes in water coverage below a ''critical value'', which appears to be less than a full monolayer of molecular water. It is suggested that the combination of molecular water at the critical value and hydroxyl groups provides complete coverage of the surface.

Acknowledgements

The authors gratefully acknowledge financial support from the Boeing Airplane Co. and the Center for Surfaces, Polymers and Colloids at the University of Washington.

References

[1] D.R. Lloyd, T.C. Ward, H.P. Schreiber (Eds.), Inverse Gas Chromatography, American Chemical Society, Washington, DC, 1989.
[2] J.K. Spelt, E.I. Vargha-Butler, in: A.W. Neumann, J.K. Spelt (Eds.), Applied Surface Thermodynamics, Marcel Dekker, New York, 1996, p. 379.
[3] J.J. Gilman, J. Appl. Phys. 31 (1960) 2208.
[4] T. Hamieh, M. Rageul-Lescouet, M. Nardin, J. Schultz, J. Chim. Phys. 93 (1996) 1332.
[5] A.I. Bailey, S.M. Kay, Proc. R. Soc. A 301 (1967) 47.
[6] E. Orowan, Z. Phys. 82 (1933) 235.
[7] W. Langel, M. Parrinello, Phys. Rev. Lett. 73 (1994) 504.
[8] M.B. Hugenschmidt, L. Gamble, C.T. Campbell, Surf. Sci. 302 (1994) 329.
[9] M.A. Henderson, Surf. Sci. 355 (1996) 151.
[10] P.J.D. Lindan, J. Muscat, S. Bates, N.M. Harrison, M. Gillan, Faraday Discuss. 106 (1997) 135.
[11] N.H. deLeeuw, S.C. Parker, Res. Chem. Intermed. 25 (1999) 195.
[12] G. Ligner, A. Vidal, H. Balard, E. Papirer, J. Colloid Interface Sci. 133 (1989) 200.
[13] G. Ligner, A. Vidal, H. Balard, E. Papirer, J. Colloid Interface Sci. 134 (1990) 486.
[14] E. Papirer, G. Ligner, H. Balard, A. Vidal, F. Mauss, Chem. Modif. Surf. 3 (1990) 15.
[15] E. Brendle, J. Dentzer, E. Papirer, J. Colloid Interface Sci. 199 (1998) 63.
[16] R.S. Mikhail, S. Brunauer, J. Colloid Interface Sci. 52 (1975) 572.
[17] E. Scholz, Karl Fischer Titration, Springer, Berlin, 1984.
[18] G.M. Dorris, D.G. Gray, J. Colloid Interface Sci. 77 (1980) 353.
[19] G.M. Dorris, D.G. Gray, J. Colloid Interface Sci. 71 (1979) 93.
[20] R.C. Reid, J.M. Prausnitz, B.E. Poling, The Properties of Gases and Liquids, McGraw-Hill, New York, 1987.
[21] J.R. Conder, C.L. Young, Physicochemical Measurement by Gas Chromatography, Wiley, Chichester, 1979.
[22] M.L. Hair, Infrared Spectroscopy in Surface Chemistry, Marcel Dekker, New York, 1967.
[23] G.M. Nishioka, J.A. Schramke, in: H. Ishida, G. Kumar (Eds.), Molecular Characterization of Composite Interfaces, Plenum Press, New York, 1985, p. 387.
[24] 71st ed., Handbook of Chemistry and Physics, CRC Press, Boca Raton, FL, 1990.